



Analysis and prediction of nonuniform deformation in composite strata during tunnel excavation

Zhuangzhuang Guo^{a,1}, Daohong Qiu^{a,1}, Yuehao Yu^a, Yiguo Xue^{a,b,*}, Qiushi Liu^a, Weimeng Zhang^a, Zhiqiang Li^{a,*}

^a Geotechnical and Structural Engineering Research Center, Shandong University, Jinan 250061, China

^b School of Engineering and Technology, China University of Geosciences (Beijing), Beijing 100083, China



ARTICLE INFO

Keywords:

Composite stratum tunnels
Nonuniform deformation classification
Numerical simulation
Deformation prediction

ABSTRACT

Due to the influence of composite strata, traditional monitoring and measurement cannot accurately reflect the nonuniform deformation and corresponding local damage to tunnels. However, the nonuniform deformation precise analysis and effective prediction of composite strata tunnels are indispensable in related projects. This analysis established a nonuniform deformation classification method and 135 groups of numerical models for a composite strata tunnel. The nonuniform deformation classification method involves four reference-defined indexes, the average deformation coefficient, variable deformation coefficient, segmental deformation coefficient, and abnormal deformation coefficient. The numerical model took the dip angle of the formation, formation proportion, in-situ stress, and pore pressure as composite strata model conditions, with four reference indexes in the nonuniform deformation classification method as the output parameters. The intelligent model of the least squares supports vector machine (PSO-LSSVM) was innovatively utilized to predict nonuniform deformation in composite strata during tunnel excavation. The prediction results of the PSO-LSSVM are consistent with actual engineering data relying on the engineering situation of Teermo Tunnel. This approach can provide targeted guidance for a composite stratum tunnel engineering evaluation system.

1. Introduction

With the increasing of tunnel projects, composite strata are frequently encountered during tunnel excavation. It is essential for predicting, preventing, and controlling the deformation of the surrounding rock of the composite formation tunnel (Jia and Tang, 2008; Yu et al., 2019). Classification of surrounding rock is essential for evaluating rock stability and selecting a tunnel support system (Li et al., 2019). The classification and prediction of nonuniform deformation of surrounding rock mainly focus on the influencing factors of deformation and seldom on complex formations (Xue et al., 2019). The accurate grading and intelligent deformation prediction in composite formations are significant for adjusting support timing, methods, and strength and ensuring tunnel construction safety (Pandit and Sivakumar babu, 2021).

The accurate classification of composite formation deformation is inseparable from the in-depth research on the deformation mechanism and classification method of soft and hard rock tunnels (Wu et al., 2004;

Do et al., 2017; Do and Wu, 2020). Grading evolution law of deformation is also widely concerned. (Zhang et al., 2019; Do and Wu, 2020; Kou et al., 2022). The layered rock mass is used as a laterally isotropic material to explain the anisotropic behavior in tunneling (Tien et al., 2006; Fortsakis et al., 2012). Further research has been conducted on the deformation and shear failure mechanism of soft and hard rock interbedding (Meng et al., 2013; Gao et al., 2014; Yang et al., 2018; Li et al., 2020; Zhou and Yang, 2021). The standard deformation classification methods are the Jethwa method (Jethwa et al., 1980), the relative strain method (Anagnostou, 1993), the Aydan method, the comprehensive coefficient method (Panthe and Nilsen, 2007) and the Hoek method (Hoek and Guevara, 2009). The main influencing factors of composite stratum tunnel construction are important for calculating tunnel deformation (Zheng et al., 2022; Di et al., 2023; Fang et al., 2023). The traditional deformation classification method mainly considers the maximum deformation, and it is difficult to determine the targeted construction of abnormal deformation area of the tunnel in composite

* Corresponding authors.

E-mail addresses: xueyiguo@cugb.edu.cn, xieagle@sdu.edu.cn (Y. Xue), zhiqiangli@sdu.edu.cn (Z. Li).

¹ Zhuangzhuang Guo and Daohong Qiu contributed equally to this work and should be considered co-first authors.

stratum (Xue et al., 2021a, 2021b).

The deformation of soft rock tunnels has always been a focus of research in theoretical analysis, experimental research, and engineering practice. However, research on the deformation nonuniformity of soft-hard rock tunnels is rare. Many scholars have conducted the evaluation methods of the soft rock tunnel deformation mainly including monitoring measurement analysis (Li et al., 2016; Yertutanol et al., 2020), numerical simulations (Tao et al., 2020; Feng et al., 2022) and physical model tests (Yang et al., 2019; Shi et al., 2021). The researchers established the engineering environment of UDEC, FLAC-PFC 3DEC numerical simulation, and numerical coupling model (Cui et al., 2014; Lin et al., 2015; Yang et al., 2018). Soft and hard rock contact zone stress-strain characteristics were selected by obtaining data sets through numerical calculation of geological models (Feng et al., 2012; Li et al., 2014). For example, the simulation results reflected the influence of the inclination of surrounding rock on tunnel deformation (Yang et al., 2019). Geomechanically model tests were conducted to analyze the failure mechanisms in soft-hard interbedded rock strata at angles 0, 45, and 90 and deformation behavior in composite strata with different strength ratios (He et al., 2010a, 2010b, 2011; Shi et al., 2021). However, there are unavoidable errors in theoretical analysis, numerical simulation, physical model test and actual tunnel engineering.

Machine learning can eliminate the influence of human factors and reveal highly nonlinear mapping relationships between input and output, making it more suitable for engineering applications (Li et al., 2020). The support vector machine dynamic prediction model of tunnel convergence during excavation has achieved good results (Mahdevari et al., 2013; Shi et al., 2019). A rapid identification method is proposed to classify and predict large deformations during tunnel construction (Liu et al., 2022). In addition, researchers compared and evaluated the Gaussian process, SVM, and wavelet neural network algorithms (He et al., 2020). The expert systems and nonlinear methods provide new approaches to solve this complex engineering problem (Bai et al., 2021). Based on rough set and extension theories, scholars focused on quantitatively analyzing each influencing factor and established a deformation grade prediction model (Xue et al., 2021a, 2021b). Concurrently, the nonuniform deformation and the BPNN deformation prediction model

were classified using the surrounding rock information of soft rock tunnel excavation (Xue et al., 2022). Most of the above studies examining overall tunnel deformation have been conducted in soft rock tunnels with single lithologies.

Since the traditional tunnel deformation classification method cannot accurately reflect soft-hard interbedded rock deformation conditions. Firstly, this study established a quantitative classification standard for nonuniform deformation in composite stratum tunnels. Secondly, a composite stratum deformation data set was obtained using numerical simulation, considering the dip angle, proportion, in-situ stress, and pore water pressure. Thirdly, deformation coefficient data were collected from the Teermo Tunnel and numerical simulation results. Finally, the PSO-LSSVM model took the dip angle of the formation, formation proportion, in-situ stress, and pore pressure as inputs, with four reference indexes in the nonuniform deformation classification method as the output parameters. A flowchart of analysis and prediction of nonuniform deformation in composite strata tunnels is shown in Fig. 1.

2. Overview of the composite strata tunnel

2.1. Geology condition

This study relies on the Teermo Tunnel of the New Chengdu Kunming Railway. It is located in Liangshan Yi Autonomous Prefecture, Sichuan Province, China. The total length of the Teermo tunnel in the study site is 6514 m, and the designed cross-sectional area is 115 m². The maximum buried depth of the tunnel is 625 m, and the natural slope is approximately 5-60°. According to the cross-section classification standard of the International Tunnel Association, it is a super-large-section tunnel. The longitudinal section of the tunnel strata is shown in Fig. 2.

The tunnel is located in a tectonic eroded valley landform, where the Niger River is deeply incised, and the ground elevation is 1050–1660 m. The tunnel is on a single-sided slope, and the terrain is high on the left and low on the right. The strata in the survey area are generally deflected, and the dip angle of the strata changes significantly. The attitude of the rock formation gradually transitioned from N8°W/57°N

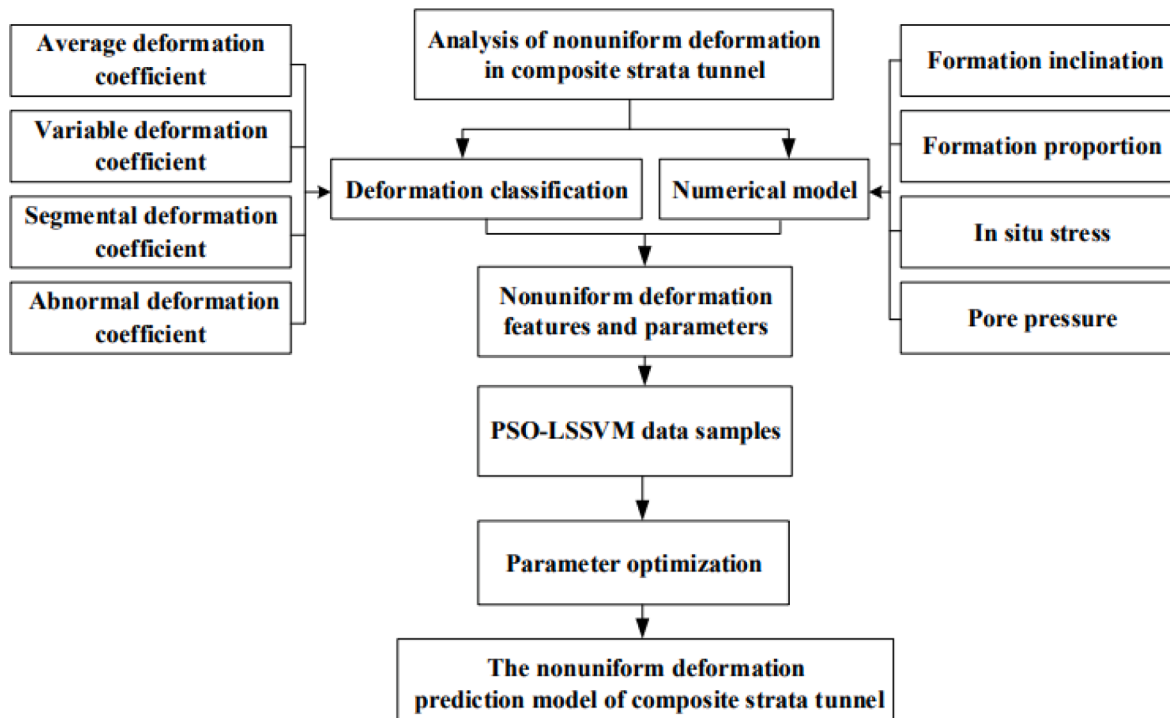


Fig. 1. Flowchart of nonuniform deformation analysis and prediction in composite strata tunnels.

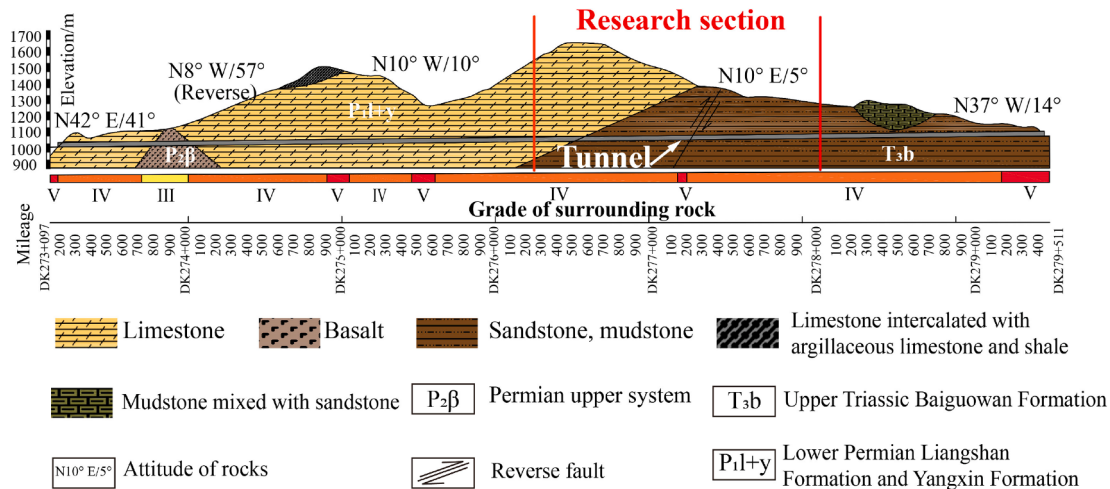


Fig. 2. Longitudinal section of the tunnel strata containing the research section.

at the tunnel entrance to N10°W/40°N and N10°W/30°N and returned to N25–37°W/22–35°N at the tunnel exit. Table 1 lists the strata information of the soft rock tunnel. The surface water in the tunnel site area is mainly the Niger River at 800–1500 m on the right side of the line, followed by ditch water and pond water, which varies significantly with seasons. The groundwater is mainly bedrock fissure water and karst water.

2.2. Construction situation

The tunnel excavation methods included the two-bench, three-bench, and three-bench plus a temporary invert excavation method. The tunnel adopted a composite lining, full-ring steel arch frame or steel arch frame, locking foot bolts, radial combined hollow bolts and grouting bolts, and annular steel mesh. Tunnel vaults were grouted with tube sheds or small conduits and filled with shotcrete. During tunnel construction, composite strata appeared on the tunnel face. The surrounding rock was mudstone and dolomite (Fig. 3a). The soft and hard surrounding rock of different strata at the tunnel face varied greatly (Fig. 3b). Table 1 lists the strata information of the soft rock tunnel. During construction, the tunnel experienced severe nonuniform deformation, and serious cracking and landslides occurred (Fig. 3). These issues prompted severe safety concerns.

3. Analysis of the nonuniform deformation of composite strata tunnels

3.1. Nonuniform deformation classification

Owing to the prominent nonuniform characteristics of tunnel deformation in composite strata, the effectiveness of the traditional monitoring method of measuring points was limited because it can only reflect the deformation of Vault, Upper convergence, Lower convergence measuring lines. Therefore, this study proposed a nonuniform deformation classification method for composite strata tunnels. According to the difference between the initial tunnel excavation and the tunnel section scanning data, the complete deformation data of the composite stratum tunnel section could be obtained. Tunnel section division diagram (Fig. 4) based on nonuniform deformation classification in dolomite-mudstone composite strata.

This study proposed a new classification method, including the average deformation coefficient $\bar{\varepsilon}$, variable deformation coefficient ξ , segmental deformation coefficient ζ , and abnormal deformation coefficient ψ to replace the traditional deformation evaluation index. Each deformation coefficient in this method based on the cumulative deformation after the composite strata tunneling. According to the average and variable deformation coefficient prediction, the excavation method and primary support strength can be optimized, respectively. The segmental deformation coefficient and abnormal deformation coefficient provide a reference to determine the scope of local strengthening support.

The formula for calculating the average deformation coefficient $\bar{\varepsilon}$ is as follow:

$$\bar{\varepsilon} = \frac{\int_0^L \delta(l) dl}{LR} \quad (1)$$

where L is the circumferential length of the tunnel (excluding the inverted arch); $\delta(l)$ is the tunnel deformation function, characterized by the distance between the actual section of the tunnel at the corresponding location and the initial section; and R is the initial radius of the tunnel. The initial radius in this manuscript is obtained by analyzing the data of the tunnel full section scanning map.

When determining whether to strengthen the tunnel support, selecting an index to measure the uneven deformation of the section and determining the proportion of the encroachment deformation is necessary. Based on this, the inhomogeneous deformation coefficient was defined as ξ , and the calculation formula is as follows:

Table 1
Strata information.

Strata	Lithology	Thickness (m)
Gravel soil (Q ₂ + 3)	grey, brown, intense weathering, rigid plastic, III hard soil	5~40
Mudstone (J _{2y})	purple, yellow-gray, silty clay filling, IV soft stone, average UCS < 12 MPa	2~6
Sandstone (T ₃ b)	yellow-gray, gray, joint fracture, weathered zone, mud sand filling, IV soft stone, average UCS = 12 MPa	2~10
Dolomite	gray white, brittle and hard, III hard stone, average UCS > 30 MPa	10~15
Basalt (P ₂ β)	dark gray, gray-green, dense, porphyritic, V sub hardstone, average UCS = 30 MPa	5~15
Limestone (P ₁ l + y)	light gray, gray, more karst developed, IV soft stone, average UCS = 20 MPa	>12

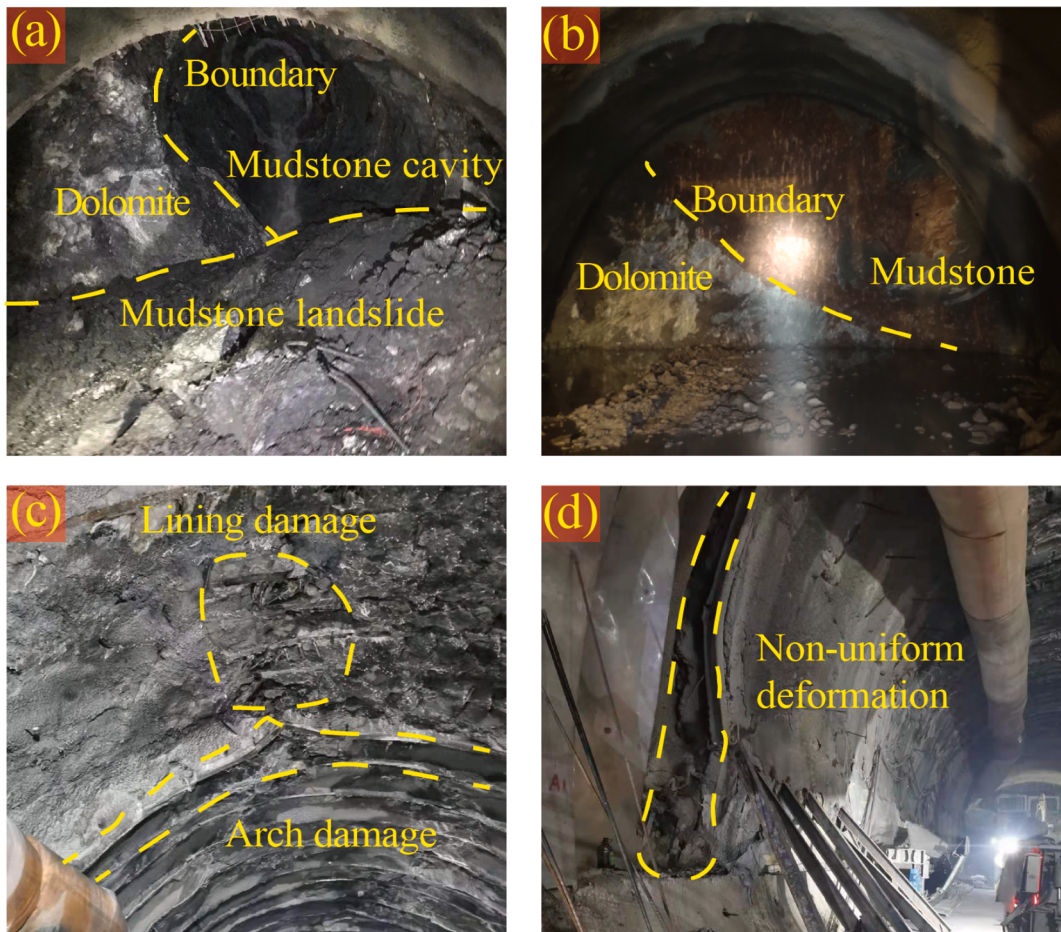


Fig. 3. Photographs of the construction sites (a) Composite strata appeared on the tunnel face and mudstone landslide. (b) The soft and hard surrounding rock of different strata at the tunnel face varied greatly. (c) Cracking in the vault and the lining of the tunnel. (d) Construction optimization measures: strengthening support in the tunnel.

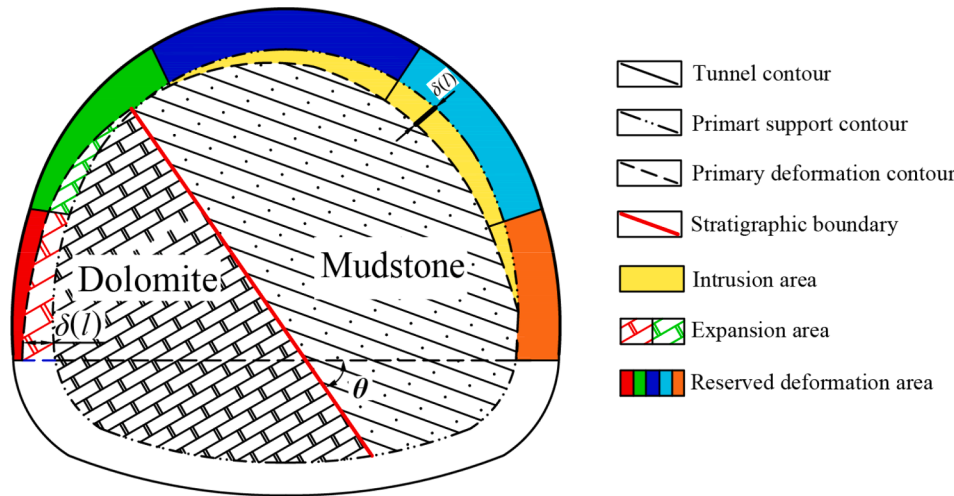


Fig. 4. Tunnel section division diagram based on the nonuniform deformation classification in dolomite-mudstone composite strata. Noted: Stratigraphic boundary line divides the formations and θ represents the stratigraphic inclination. The intrusion area (yellow) represents the deformation intrusion of the rock mass after excavation. The expansion area (dashed) represents the over-excavated rock mass exists insufficient deformation and support detachment. $\delta(l)$ is the tunnel deformation function, characterized by the distance between the actual section of the tunnel at the corresponding location and the initial quote. The tunnel's normal reserved deformation area is divided into five different color areas: the left sidewall (red), the left arch waist (green), the vault (blue), the right arch waist (cyan), and the right sidewall (orange).

$$\xi = \frac{S_{int}}{S_{int} + S_{exp}} = \frac{\sum_1^{n_1} \int_0^{l_{n_1}} \delta_1(l) dl}{\sum_1^{n_1} \int_0^{l_{n_1}} \delta_1(l) dl + \sum_1^{n_2} \int_0^{l_{n_2}} \delta_2(l) dl} \quad (2)$$

where S_{int} and S_{exp} are the encroachment and expanded area of the section; n_1 and n_2 are the number of cross-section encroachment and expansion areas; l_{n_1} and l_{n_2} are the arc length of the section encroach-

ment and outward expansion; and $\delta_1(l)$ and $\delta_2(l)$ are the deformation function of the section encroachment and outward expansion.

The tunnel section was divided into five parts to obtain the location of the abnormal encroachment deformation: the left sidewall, the left arch waist, the vault, the right arch waist, and the right sidewall (Fig. 4). When ideas for strengthening the support are provided, the calculation formula of the piecewise deformation coefficient ζ is as follows:

$$\zeta_n = \begin{cases} \frac{\bar{\delta}_{n_{int}} + d}{R_n} & (\text{All intrusions}) \\ \frac{d - \bar{\delta}_{n_{exp}}}{R_n} & (\text{All expansions}) \\ \frac{\bar{\delta}_{n_{int}} - \bar{\delta}_{n_{exp}} + d}{R_n} & \left(\begin{array}{l} \text{Both encroachment} \\ \text{and expansion parts} \end{array} \right) \end{cases} \quad (3)$$

where $\bar{\delta}_{n_{int}}$ and $\bar{\delta}_{n_{exp}}$ are average encroachment limit and amount of expansion in the corresponding area, R_n is the equivalent tunnel radius of the corresponding area and d is reserve deformation for the tunnel.

After obtaining the deformation of each segment, there may be encroachment deformation in some areas. Therefore, the abnormal deformation coefficient is set for local key deformation areas. It provides precise guidance for the decision of specific support in the encroachment deformation areas after the overall deformation level of the tunnel is determined. Adding this parameter to the technical method proposed in this paper greatly improves the efficiency of risk prevention and control and engineering governance under complex geological conditions. For this reason, an abnormal deformation coefficient ψ was defined, and the calculation formula is as follows:

$$\psi = \frac{S_{int}}{L_{int}} = \frac{\int_0^{L_{int}} \delta(l) dl}{L_{int}} \quad (4)$$

where L_{int} indicates the arc length corresponding to the intrusion limit.

Based on the actual situation of the Teermo tunnel, the degree of deformation of each index was divided into five grades from I to V (Aydan et al., 1996; Li et al., 2016), as shown in Table 2.

3.2. Field-measured data set acquisition

First, accurate monitoring data of the vault settlement and horizontal convergence of the Teermo tunnel section were obtained. The deformation development trend in real-time is shown in Fig. 5. However, there are certain limitations in analyzing the nonuniform deformation of a composite stratum tunnel. Therefore, the geological sketch and full-section scan data were further extracted, as shown in Fig. 6.

The establishment of the tunnel sample dataset is based on the measured deformation data of tunnel monitoring. According to the classification method proposed in Section 3.1, the four coefficients in the abnormal deformation classification and the relative deformation amount of the five deformation areas are divided and judged. After that, the dataset was contained with the deformation coefficients and deformation level of each abnormal deformation area. Field-measured data sets aren't easy to reflect the influence of different factors on the deformation fully. Therefore, we used numerical simulations to acquire and enrich the data set in this study.

3.3. Numerical model data set acquisition

3.3.1. Model establishment and parameter determination

The numerical simulation software FLAC3D is used to model and calculate the Teermo tunnel. According to the range of disturbance in the tunnel excavation, the distance from the left and right sides of the tunnel excavation outline to the boundaries was set to be three times the

Table 2

Grading of various deformation coefficients.

Grade	$\bar{\varepsilon}$ (%)	ξ	ζ (%)	ψ (cm)
I	$\bar{\varepsilon} \leq 2$	$0 < \xi \leq 0.9$	$\zeta \leq 2$	$0 < \psi \leq 5$
II	$2 < \bar{\varepsilon} \leq 4$	$0.9 < \xi \leq 0.92$	$2 < \zeta \leq 4$	$5 < \psi \leq 10$
III	$4 < \bar{\varepsilon} \leq 6$	$0.92 < \xi \leq 0.94$	$4 < \zeta \leq 6$	$10 < \psi \leq 15$
IV	$6 < \bar{\varepsilon} \leq 8$	$0.94 < \xi \leq 0.96$	$6 < \zeta \leq 8$	$15 < \psi \leq 20$
V	$\bar{\varepsilon} > 8$	$0.96 < \xi \leq 1$	$\zeta > 8$	$\psi > 20$

tunnel span. The design tunnel span was 14 m, the burial depth was 90 m upwards, 30 m downwards, 32 m along the tunnel axis, and the model was 120 m wide. The drilling and blasting method were adopted for construction, and the three-step method was used for excavation. The heights of the three steps were 3.15 m, 4.1 m, and 2.5 m from top to bottom, and the excavation footage per cycle was 2 m. Diagram of dimension of tunnel and schematic diagram of three-bench excavation method, as shown in Fig. 7(a) and Fig. 7(b).

In this study, deformation monitoring points were set up at the top of the vault, the upper stair arch, the central stair arch, the lower stair arch, and the bottom of the inverted arch. The displacement boundary condition sets the usual constraints to limit horizontal displacement. It sets fixed constraints at the bottom of the model, leaving the upper boundary of the model unconstrained. The seepage boundary condition sets the surroundings and bottom of the numerical model. The boundary was set as an impermeable boundary, and the initial pore water pressure of the model was the hydrostatic pressure of the formation, which was proportional to the burial depth. During the tunnel excavation process, the pore water pressure of the tunnel face was fixed at zero. The Mohr-Coulomb model was used to simulate the mechanical behavior. However, the main concern was stratum difference of composite tunnel. The rock's behavior under these in-situ stress is simplified appropriately in the course of the study. Future research will focus on physical and mechanical properties, and the mechanical behavior of the rock. The calculation parameters of the surrounding rock and support in the numerical model were determined according to the engineering site investigation and design data. The modeling process was simplified when the support for the steel arch function was considered. The parameters are shown in Table 3. All indicators in these finite difference models have been validated. The post-processing results of the model are basically consistent with the monitoring data of engineering samples.

3.3.2. Determination of numerical model influencing factors

Studying the nonuniform deformation in composite strata requires understanding the influence of numerical model influencing factors on the target value. This study explained in detail the reasons for selecting the dip angle, proportion, in-situ stress, and pore water pressure (Jia and Tang, 2008; Yu et al., 2019). Scholars focused on quantitatively analyzing each influencing factor and established a deformation grade prediction model (Xue et al., 2021a, 2021b). Geomechanically model tests were conducted to analyze the failure mechanisms in soft-hard interbedded rock strata at angles 0, 45, and 90. (He et al., 2010a, 2010b, 2011; Shi et al., 2021).

According to the extensive research by experts and the geological conditions of burial depth and groundwater conditions of the Teermo tunnel, this research selected the formation dip angle, proportion, in-situ stress and pore pressure at different levels for numerical modeling. This model analyzed the deformation characteristics of rock formations with specific dip angles about 0°, 45°, 90°, 135°, 180°. The schematic diagram of the division of dip angles and proportions is shown in Fig. 4.

According to the above division of the dip angle, proportion, in-situ stress, and water pressure of the formation boundary, several factors were combined to establish 135 sets of numerical models. Selected model parameters are shown in Table 4. The proportion of strata was divided into three distinct proportions of soft rock and hard rock: 1:1, 1:2, and 2:1. The applied in-situ stress was divided into three levels: 0 MPa, 4 MPa, and 8 MPa. The groundwater situation was realized by adjusting the pore water pressure to three levels: 0 MPa, 0.5 MPa, and 1 MPa. Numerical simulation grouping under different working conditions was established, as shown in Fig. 7(c). The green part is the soft rock area represented by sandstone, and the blue part is the hard-rock area represented by dolomite. The upper and lower strata proportions changes through the inclination angle of the boundary line. It can achieve the simulation of complex working conditions of different in-situ stresses in the composite strata.

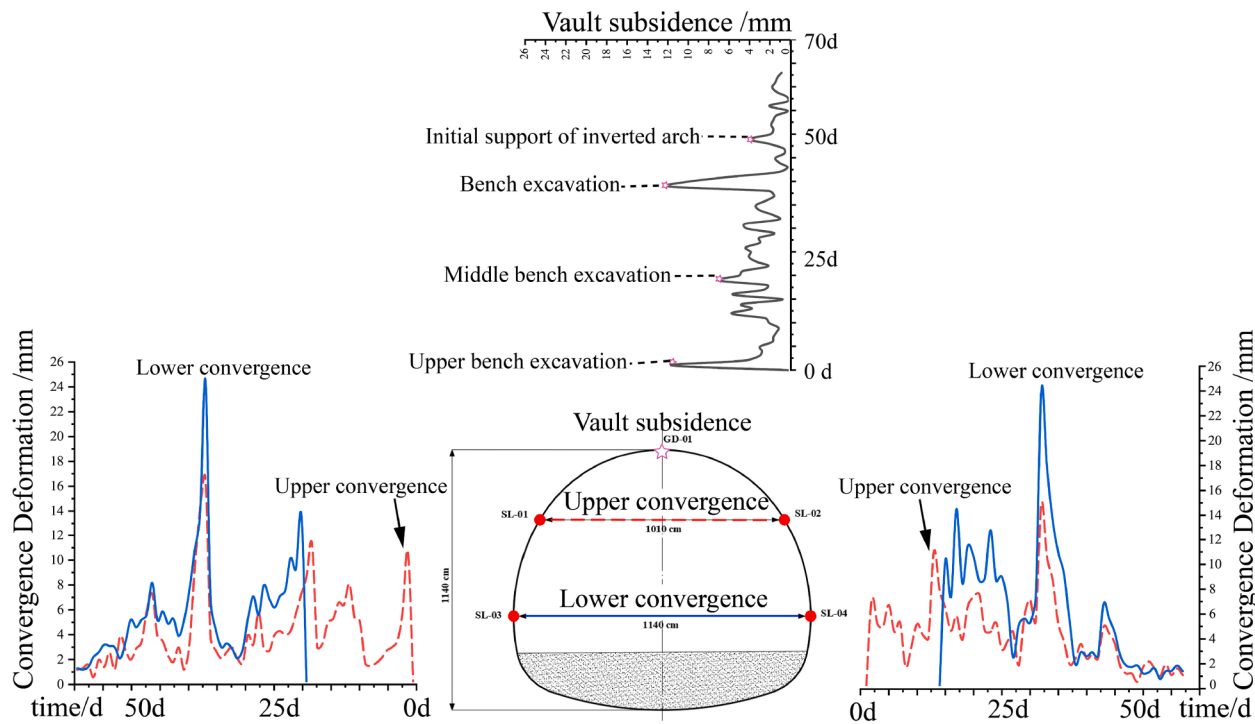


Fig. 5. Traditional section monitoring measurement data in the different areas (Vault, Upper convergence, Lower convergence).

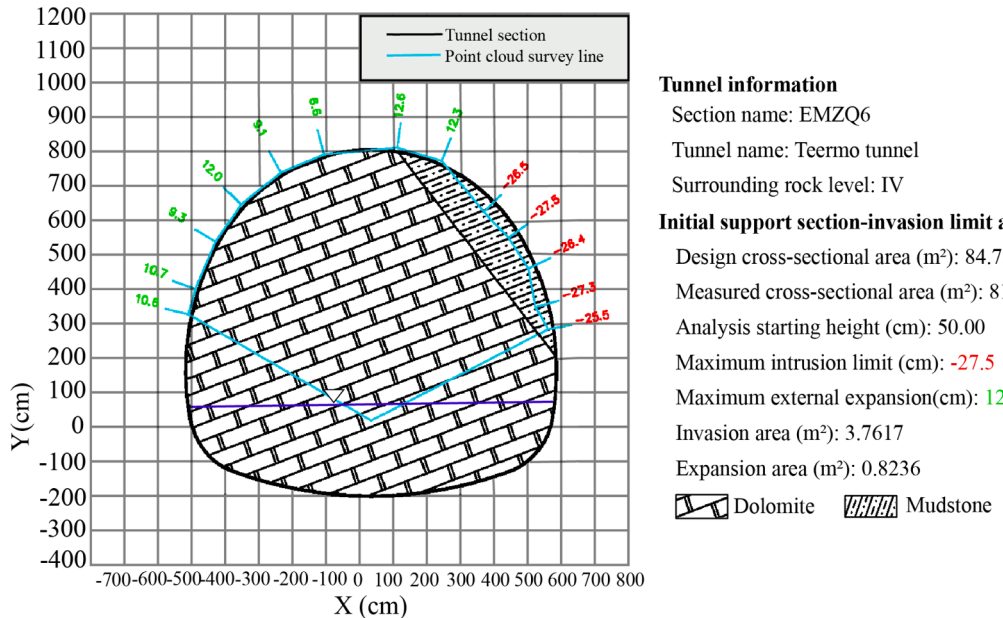


Fig. 6. Geological sketch map and scanning map of the entire section. Scan curves can reflect the tunnel deformation function, characterized by the distance between the actual section of the tunnel at the corresponding location and the initial section.

3.3.3. Model reliability verification

The accuracy of the numerical model was verified by comparing the numerical simulation results with the on-site monitoring measurement data. The comparison results are shown in Table 5. In general, the deformation error of all sections shall not exceed 10%. The comparison shows that the numerical simulation results are closer to the on-site monitoring data.

3.3.4. Numerical model data set acquisition

The extracted cross-sectional deformation data of 135 models in the

numerical simulation were brought into the classification method described in subsection 3.1. The composite stratum tunnel surrounding the sample set was established to provide a data reference for subsequent index classification (Table 6). The surrounding rock deformation prediction sample set of the composite stratum tunnel collated and summarized the data of 135 numerical models in the numerical simulation. And then, the study took the deformation grade of each index as the output.

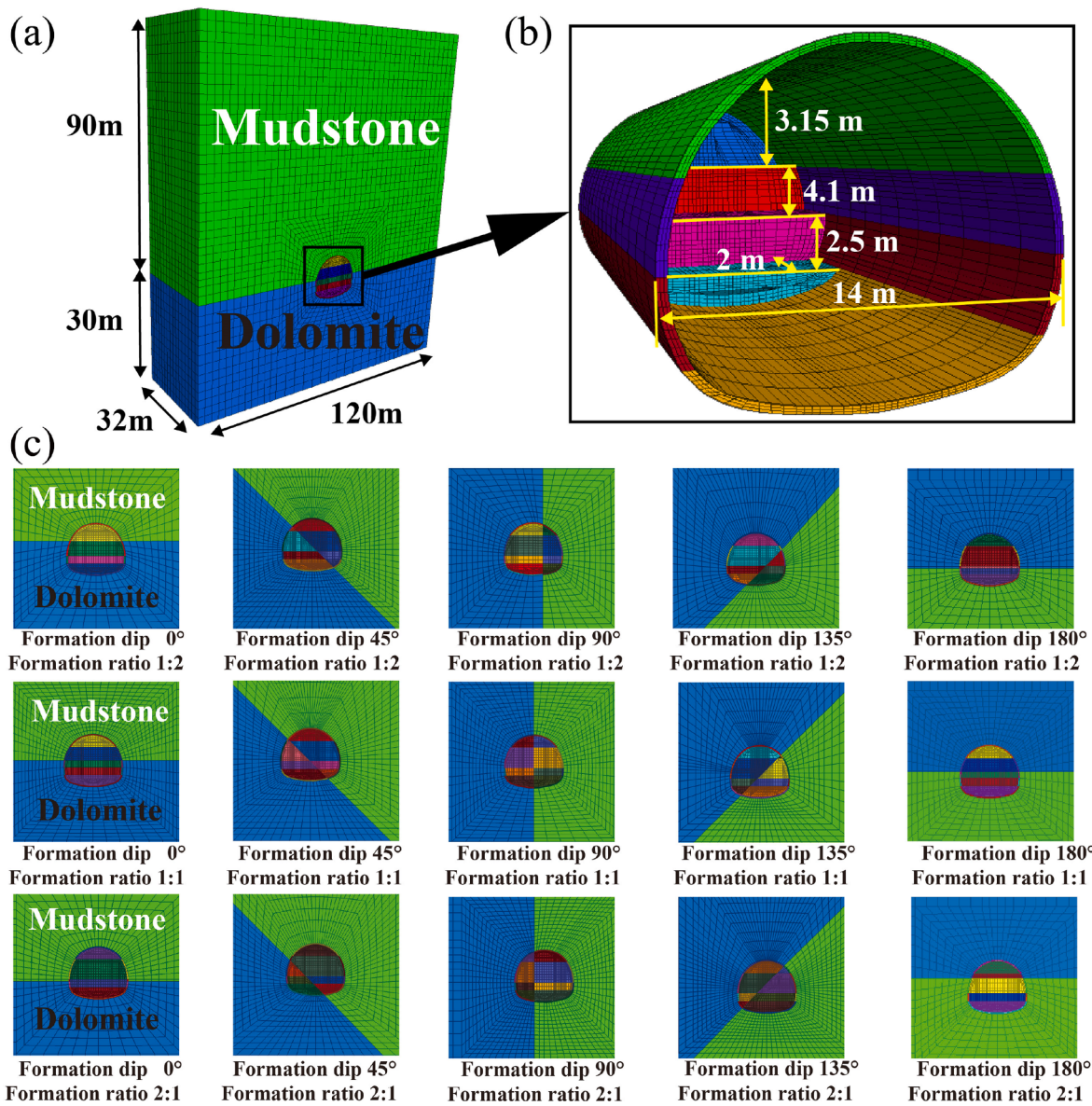


Fig. 7. Numerical model diagram. (a) Diagram of dimension of tunnel and strata. (b) Schematic diagram of three-bench excavation method. The heights of the three steps were 3.15 m, 4.1 m, and 2.5 m from top to bottom, and the excavation footage per cycle was 2 m. (c) The blue grid represents the dolomite and the green grid represents the mudstone. In different stratigraphic inclinations and proportions, tunnel faces are divided and monitored according to each excavation step and excavation area zoning.

Table 3
Numerical modeling parameter determination.

	Volume weight (kg/m^3)	Internal friction angle ($^\circ$)	Cohesive force (MPa)	Permeability coefficient (cm/s)	Poisson's ratio (μ)	Elastic modulus (GPa)	UCS (MPa)	Tensile strength (MPa)
Dolomite	2694.6	40.7	16.81	8.7×10^{-9}	0.21	55.73	62.69	10.05
Mudstone	2399.3	24.6	2.3	8.6×10^{-5}	0.37	3.8	3.26	0.51
Joint plane	2450	–	–	–	–	40	–	–

4. Prediction of the nonuniform deformation with PSO-LSSVM

4.1. PSO-LSSVM theory

The particle swarm algorithm (Blackwell and Kennedy, 2019) is an optimization method based on swarm intelligence. Particle swarm optimization (PSO) finds the optimal solution to a problem through cooperation and information sharing among individuals in the swarm

(Das et al., 2022). Therefore, using the particle swarm algorithm to determine the optimal parameters can ensure the accuracy of the prediction model.

The PSO algorithm considers the D-dimensional space, with n particles, where the position of the ith particle may be described as $X_i = (x_{i1}, x_{i2}, \dots, x_{iD})^T$. The velocity of the ith particle is defined as $V_i = (v_{i1}, v_{i2}, \dots, v_{iD})^T$ where the individual extrema of the ith particle are $P_i =$

Table 4
Formation parameter table of numerical models.

No.	Inclination (°)	Proportion	Ground stress (MPa)	Pore pressure (MPa)
1	0	1:1	0	0
2	0	1:2	0	0
3	0	2:1	0	0
4	0	1:1	4	0
5	0	1:2	4	0
6	0	2:1	4	0
7	0	1:1	8	0
8	0	1:2	8	0
9	0	2:1	8	0
10	45	1:1	0	0.5
...
125	135	1:2	8	0.5
126	135	2:1	8	0.5
127	180	1:1	0	1
128	180	1:2	0	1
129	180	2:1	0	1
130	180	1:1	4	1
131	180	1:2	4	1
132	180	2:1	4	1
133	180	1:1	8	1
134	180	1:2	8	1
135	180	2:1	8	1

$(P_{i1}, P_{i2}, \dots, P_{id})^T$, and the global extremum is $P_g = (P_{g1}, P_{g2}, \dots, P_{gd})^T$.

$$V_{id}^{k+1} = \omega V_{id}^k + c_1 r_1 (P_{id}^k - X_{id}^k) + c_2 r_2 (P_{gd}^k - X_{gd}^k) \quad (5)$$

$$X_{id} = X_{id} + V_{id} \quad (6)$$

where ω is the inertia weight, which controls how much speed each

particle inherits; D is the dimension of the solution to be optimized; n is the population size, k is the current iteration number; V_{id} is the particle speed; c_1 and c_2 are the acceleration factors, which control the speed calculated; and r_1 and r_2 are two random numbers ranging between 0 and 1, which can increase the randomness of the search. The position and velocity are usually limited $[-X_{\max}, X_{\max}]$ and $[-V_{\max}, V_{\max}]$, which can prevent blind searches of particles.

In 2022, Qi et al. proposed a least squares support vector (LSSVM) federation algorithm (Qi et al., 2022). Compared with SVM, LSSVM converts inequality constraints into equality constraints and transforms quadratic programming problems into linear equation problems. At the same time, LSSVM parameter optimization and prediction are integrated into PSO algorithm. Finally, the classification decision model of LSSVM is obtained.

$$f(X_i) = \frac{1}{\sqrt{\frac{1}{n} \sum_{k=1}^n (X_k - \hat{X}_k)^2}} \quad (7)$$

n is the population size, $X = (X_1, X_2, \dots, X_n)$ is the four-dimensional vector of the average deformation coefficient, variable deformation coefficient, segmental deformation coefficient, and abnormal deformation coefficient, $f(X_i)$ is the output vector and the value is the corresponding deformation grade.

4.2. Data samples of PSO-LSSVM

Index classification was established based on grading various deformation coefficients (Table 7). PSO-LSSVM is not proposed by us. This manuscript creatively applies it to large deformation of soft rock. The complete data are in the appendix A.

Table 5

Verification of field monitoring data by numerical simulation results.

No.	Vault settlement			Convergence			Lower convergence		
	Calculation results	Actual data	Error rate	Calculation results	Actual data	Error rate	Calculation results	Actual data	Error rate
1	25.6	26.4	3.1%	20.4	22.6	10.8%	11.4	12.1	6.1%
2	17.1	18.2	6.4%	29.1	29.8	2.4%	19.1	18.5	3.1%
3	23.3	24.6	5.6%	15.6	16.2	3.8%	9.7	10.3	6.2%
4	10.3	11.3	9.7%	30.3	29.8	1.7%	25.4	27.3	7.5%
5	15.6	16.1	3.2%	29.7	33.6	13.1%	16.2	15.1	6.8%

Table 6

Sample set of composite formation tunnel.

No.	$\bar{\epsilon}$ (%)	ξ	ζ (%)						ψ (cm)
				Top arch	Left arch	Left sidewall	Right arch	Right sidewall	
1	4.17	0.94	3.90	2.20	1.23	2.20	1.23	1.23	10.77
2	3.75	0.88	2.84	1.35	0.54	4.14	3.91	3.91	9.51
3	4.34	0.95	2.69	1.51	1.08	5.71	5.61	5.61	12.21
4	3.60	0.97	2.27	1.85	1.33	3.95	4.60	4.60	6.55
5	5.96	1.00	3.93	4.22	4.86	4.22	4.86	4.86	14.73
6	5.05	0.98	4.23	3.59	1.78	3.59	1.78	1.78	12.70
7	4.64	0.93	3.66	1.80	0.55	4.66	4.40	4.40	12.44
8	4.89	0.98	3.28	1.88	1.35	5.98	5.98	5.98	14.80
9	4.18	1.00	2.58	1.93	1.64	4.71	5.24	5.24	9.04
10	6.78	1.00	4.33	5.07	5.44	5.07	5.44	5.44	18.64
...
126	8.71	1.00	7.27	6.85	3.50	6.85	3.50	3.50	25.49
127	8.29	0.97	6.70	5.05	2.27	7.92	6.12	6.12	25.23
128	8.55	1.00	6.32	5.14	3.07	9.24	7.70	7.70	27.59
129	7.83	1.00	5.61	5.18	3.35	7.97	6.95	6.95	21.84
130	10.44	1.00	7.36	8.33	7.15	8.33	7.15	7.15	31.44
131	7.05	0.94	6.26	5.19	2.81	5.19	2.81	2.81	22.92
132	6.59	0.88	5.47	4.28	2.23	7.05	5.36	5.36	21.85
133	7.76	0.95	5.25	4.56	2.83	8.54	6.81	6.81	23.90
134	6.40	0.97	4.84	4.87	3.09	6.70	5.81	5.81	18.12
135	8.54	1.00	6.37	6.49	5.26	6.49	5.26	5.26	22.84

Table 7

The deformation level of the composite formation tunnel sample set.

No.	\bar{e}	ξ	$\zeta(\%)$					ψ
			Top arch	Left arch	Left sidewall	Right arch	Right sidewall	
1	III	I	II	II	I	II	I	III
2	II	I	II	I	I	III	II	II
3	III	II	II	I	I	IV	IV	III
4	II	III	II	I	I	II	III	II
5	III	V	II	III	III	III	III	III
6	III	III	III	II	I	II	I	III
7	III	I	II	I	I	III	III	III
8	III	IV	II	I	I	IV	IV	III
9	III	IV	II	I	I	III	IV	II
10	IV	V	III	IV	IV	IV	IV	IV
...
126	V	V	V	V	II	V	II	V
127	V	III	V	IV	II	V	V	V
128	V	V	V	IV	II	V	V	V
129	IV	V	IV	IV	II	V	V	V
130	V	V	V	V	V	V	V	V
131	IV	II	V	IV	II	IV	II	V
132	IV	I	IV	III	II	V	IV	V
133	IV	II	IV	III	II	V	V	V
134	IV	III	III	II	II	V	IV	IV
135	V	V	V	V	IV	V	IV	V

4.3. Training performance of PSO-LSSVM

First, this research used the particle swarm algorithm to find the optimal penalty factor c and kernel parameter g . We calculated the numerical characteristics of group a-h according to each index in the classification method. We then iterated until the particle swarm fitness was globally optimal before stopping to obtain the optimal penalty factor c and kernel parameter g . Finally, we predicted in groups a-h in Table 8. Table 9 shows that the accuracy of the prediction results ranged from 82.86% to 94.29%. The a-h group prediction results obtained are as follows (Fig. 8):

4.4. Engineering application

The 100 groups of data were used as the training set, and the 35 groups of data were used as the test set. Fifteen samples from typical tunnel sections were selected for engineering verification of the constructed PSO-LSSVM model (Table 10). The complete data are in the attachment A. The constructed composite formation tunnel nonuniform deformation prediction model was verified based on data from these samples. The verification results are shown in Table 11.

It can be seen from the above prediction results that the PSO-LSSVM prediction results are generally good. It indicates that the model established in this study can accurately predict the deformation of composite strata tunnels and can be successfully applied to predict the nonuniform deformation of composite strata tunnels to optimize initial foundation support strength for construction personnel. It may also provide a reference for determining the scope of local strengthening support.

Table 8
PSO-LSSVM model parameter table.

Group	n	D	k	V_{id}	c	g
a	50	0.95	100	25	241.7298	1.3671
b	100	0.95	100	25	277.0058	1.3437
c	50	0.95	100	25	207.0867	0.69656
d	100	0.95	100	25	203.3519	1.7134
e	100	0.95	100	25	212.6252	1.3108
f	100	0.95	100	25	193.8824	1.1023
g	100	0.95	100	25	203.5724	1.0119
h	100	0.95	100	25	212.6252	1.3108

5. Discussions

5.1. Compared with engineering classification criteria

The on-site construction classified the tunnel with large extrusion deformation, referred to the railway tunnel design code (TB10003), and determined the significant deformation classification standard in Table 12.

Comparing the engineering classification method with the method proposed in this study, the deformation classification method proposed in Table 2 divides the risk level from three to five, providing an accurate reference for determining tunnel excavation methods and support strength. The overall deformation of the face is accurately divided into five regions, which provides a reference for determining support methods and strengths at different positions. At the same time, the actual grading method in engineering is considered the dip angle of the formation boundary and formation proportion. The classification method in this study is more detailed in terms of inclination angle and proportion. It simultaneously increases the consideration of in-situ stress and pore water pressure, verified in the numerical simulations. The above comparative analysis showed that the method proposed in this study had high accuracy and applicability.

5.2. Compared with other machine learning models

As described in section 4.4, the 35 groups of data were used as the test set. The PSO-LSSVM model applied to this study was compared with the other machine learning prediction models, including the support vector machine model (SVM model), the backpropagation neural network model (BPNN model) and the algorithms model about the backpropagation neural network model based on genetic algorithm (GA-BPNN model). The existing cases were used as learning samples, and the comparison results are shown in Table 13. The PSO-LSSVM model has a high prediction accuracy. As shown in Tables 9 and 11, the performance of the PSO-LSSVM model proposed in this paper was the best on the training and test sets, with correct rates of 94.29% and 93.33%, respectively. However, the PSO-LSSVM prediction model database only considers the changes in composite formation parameters in the tunnel face. The longitudinal geological changes along the tunnel axis also affect its deformation characteristics, so the model accuracy is only higher than 80% in some aspects.

5.3. Guidance and application in engineering

The surrounding rock is weak and fractured for the composite stratum tunnel in this study area. When the deformation is too large, if the second lining is applied when the deformation is stable, the primary flexible support cannot provide sufficient supporting strength. After the deformation results are obtained in the preliminary survey stage of the actual project, selecting the appropriate support method and the scope of local strengthening support is necessary. The new Austrian tunneling method (NATM) uses primary shotcrete and flexible support according to traditional grading and construction guidance. The full-section method is used for the average deformation grades I, II and III; the weak blasting is used. The two and three steps excavation can be used when the deformation grades IV and V need to be excavated by subsections and adopt non-blasting excavation construction.

Comparing the engineering method of NATM with the method proposed in this study, the average deformation coefficient \bar{e} determine reserved deformation and support parameters before excavation. After obtaining the excavated data, the variable deformation coefficient ξ can be corrected to provide more accurate reserved deformation and support parameters to guide the work in the next stage. Owing to the prominent nonuniform characteristics of tunnel deformation in composite strata, the segmental deformation coefficient ζ and abnormal deformation coefficient ψ replace the traditional deformation evaluation index. When

Table 9
Model prediction validation results.

	$\bar{\epsilon}$	ξ	Ψ	ζ	Top arch	Left arch	Left sidewall	Right arch	Right sidewall
Accuracy	85.17%	82.86%	91.43%		91.43%	88.57%	94.29%	88.57%	91.43%

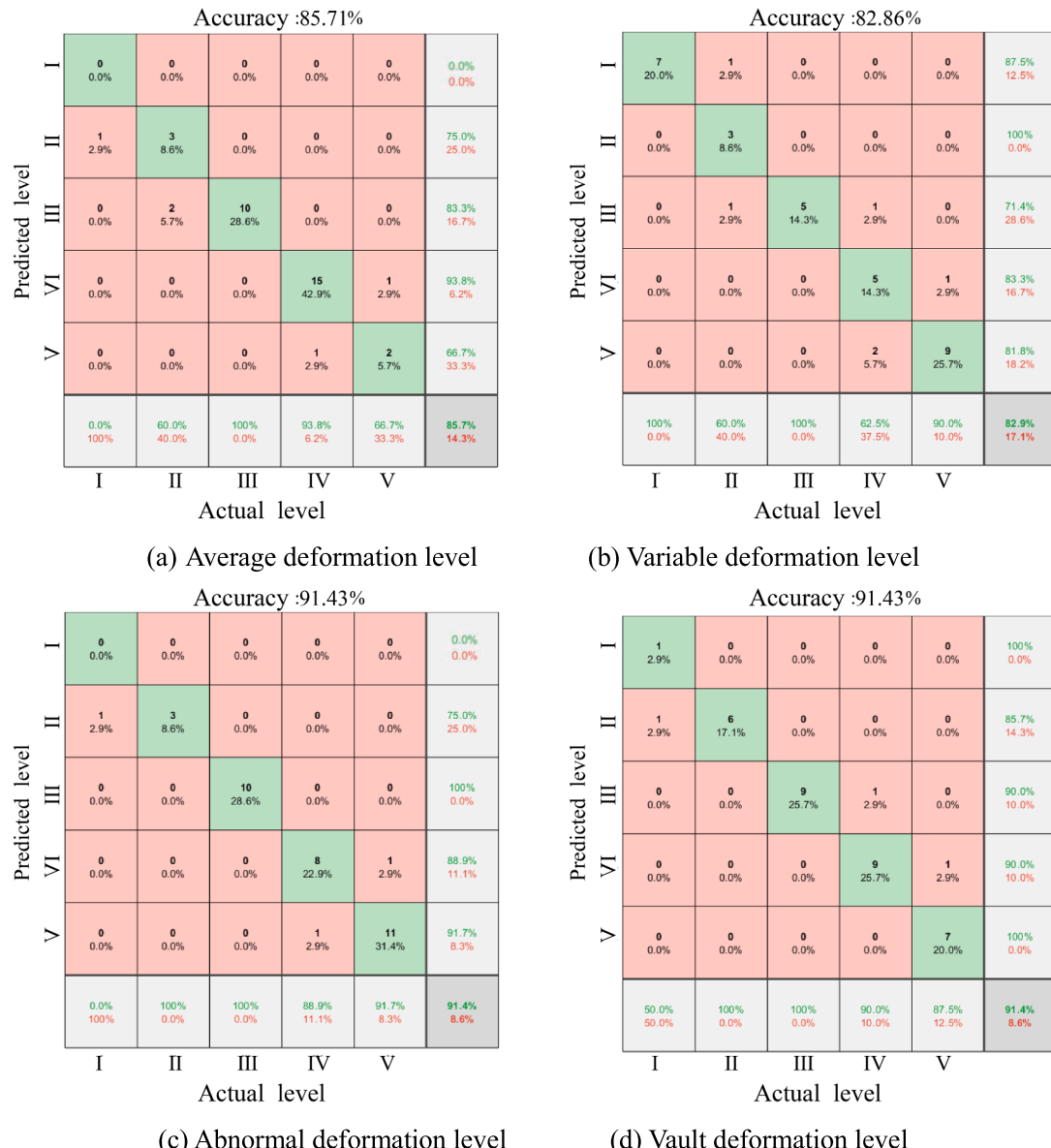


Fig. 8. Prediction results of each deformation coefficient. Here, the green area is the array of predictions correctly and reflects the accuracy of the model at each level.

anchor and grouting support are carried out in an area with classification for uneven and abnormal deformation, the length and number of the anchor and grouting material and technology should be reasonably chosen. Because of these problems, we will conduct a follow-up study.

6. Conclusions

Given the shortcomings of the traditional tunnel deformation classification method in nonuniform deformation, this research proposed a novel nonuniformity classification method and established the PSO-

LSSVM deformation intelligent prediction model. Based on the Teermo Tunnel, this study obtained accurate deformation levels and model prediction results and drew the following conclusions:

- Given that traditional monitoring and measurement data cannot reflect the nonuniform deformation of a composite stratum tunnel, this study improved the classification method based on the tunnel deformation monitoring method. The average deformation coefficient, variable deformation coefficient, segmental

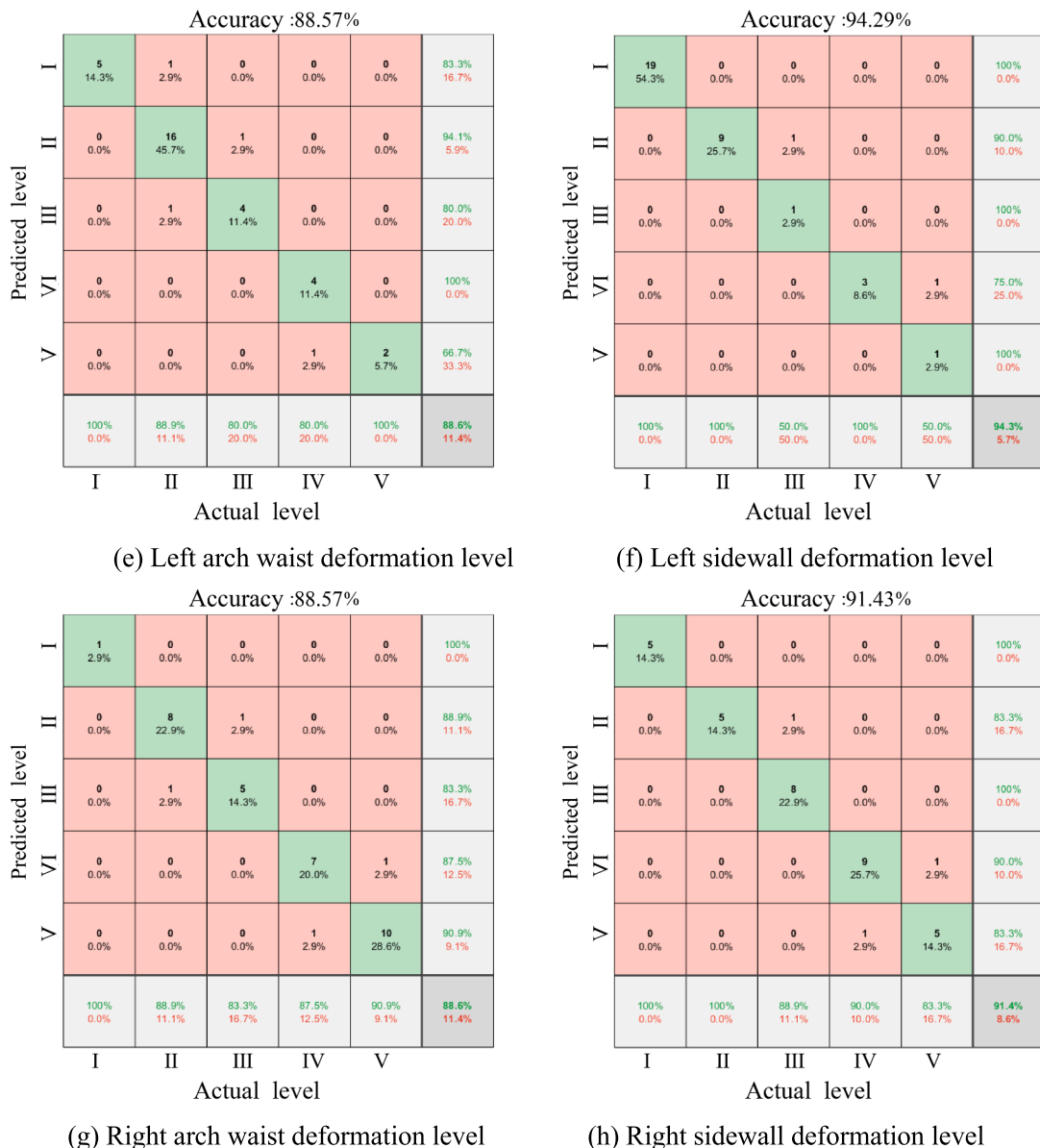


Fig. 8. (continued).

Table 10
Typical tunnel sections dataset classification table.

No.	$\bar{\varepsilon}$	ξ	ζ	Ψ				
				Top arch	Left arch	Left sidewall	Right arch	Right sidewall
1	IV	V	III	III	II	III	III	III
2	III	II	III	II	I	II	I	IV
3	IV	V	IV	II	I	II	I	IV
4	V	V	IV	III	II	V	IV	V
5	IV	V	IV	III	II	III	II	V
6	V	V	IV	IV	III	IV	III	V
7	III	II	III	II	I	II	III	III
8	IV	I	III	II	II	IV	III	V
9	IV	V	III	II	II	IV	IV	V
10	IV	V	IV	III	II	III	II	IV
11	III	V	III	II	I	III	III	III
12	III	II	II	II	I	II	I	III
13	II	II	II	I	I	II	II	II
14	III	V	III	II	I	IV	III	IV
15	III	V	II	II	I	IV	IV	IV

deformation coefficient, and abnormal deformation coefficient were defined to determine the deformation level.

- The 135 numerical deformation monitoring points data set up in the numerical simulation were sorted and summarized. After that, it summarized the variation law of the nonuniform deformation index of the tunnel under the influence of specific stratum parameters. And the deformed dataset is applied to prediction model training and engineering practice verification.
- Using the PSO-LSSVM algorithm, a prediction model for rock deformation surrounding composite strata tunnels was established. Model accuracy was verified using field-measured data. The prediction accuracy is up to 94.29%, indicating that the model achieved good predictions. Compared with engineering classification criteria, the composite stratum tunnel's deformation classification method and prediction model can provide a real-time update and dynamic monitoring. It can also accurately predict the deformation of the tunnel and provide a reference for construction personnel to optimize the initial foundation support strength and determine the local strengthening support range.

Table 11

Typical tunnel sections prediction results.

	$\bar{\varepsilon}$	ξ	Ψ	ζ				
				Top arch	Left arch	Left sidewall	Right arch	Right sidewall
Accuracy	93.33%	86.67%	93.33%	86.67%	80.00%	93.33%	80.00%	93.33%

Table 12

Large deformation classification standard based on the code for design of railway tunnel (TB10003).

Grade	Relative deformation	Bedding type	Cataclastic type		Fault type	
			Along structural line	Unfavorable structural line	Along structural line	Unfavorable structural line
I	3% ~ 5%	< 20%	0	< 20%	0	< 20%
II	5% ~ 8%	20 ~ 40%	< 20%	20 ~ 40%	< 20%	20 ~ 40%
III	> 8%	> 40%	> 20%	> 20%	> 20%	> 40%

Note: The code for design of railway tunnel (TB10003) was published in China. The relative deformation is the ratio of the deformation to the equivalent radius of the tunnel. Bedding type refers to the included angle between the axial direction of the tunnel and the strike of the rock stratum being less than 45°. Along structural line means that the included angle between the axial direction of the tunnel and the structural line is less than 45°. The percentages refer to the weak layer's proportion.

Table 13

The prediction results of the four models.

Model	$\bar{\varepsilon}$	ξ	Ψ	ζ				
				Top arch	Left arch	Left sidewall	Right arch	Right sidewall
SVM	71.43%	71.43%	77.14%	85.71%	77.14%	85.71%	82.86%	85.71%
BPNN	68.57%	80.00%	74.29%	80.00%	71.43%	82.86%	85.71%	77.14%
GA-BPNN	74.29%	91.43%	82.86%	74.29%	80.00%	88.57%	91.43%	80.00%
PSO-LSSVM	85.71%	82.86%	91.43%	91.43%	88.57%	94.29%	88.57%	91.43%

(4) The dataset of heterogeneous deformation of the composite stratum tunnel constructed in this study was obtained by numerical simulation of the Teermo tunnel and had specific regional characteristics. In the future, we can extensively refer to the composite stratum tunnel projects with specific geological characteristics in other regions and continuously enrich the data sample set of composite stratum tunnel nonuniform deformation. It will allow for establishing a widely applicable composite stratum tunnel nonuniform deformation evaluation system.

CRediT authorship contribution statement

Zhuangzhuang Guo: Conceptualization, Data curation, Writing – original draft. **Daohong Qiu:** Writing – review & editing, Visualization. **Yuehao Yu:** Software, Methodology. **Yiguo Xue:** Resources, Funding acquisition, Supervision, Validation. **Qiushi Liu:** Investigation, Data curation. **Weimeng Zhang:** Investigation, Formal analysis. **Zhiqiang Li:** Funding acquisition, Validation.

Declaration of Competing Interest

The authors declare that they have no known competing financial interests or personal relationships that could have appeared to influence the work reported in this paper.

Data availability

Data will be made available on request.

Acknowledgments

Research in this paper is supported by the National Natural Science Foundation of China (grant numbers 42293351, 41877239, 51422904 and 51379112), and Shandong Provincial Natural Science Foundation (grant number ZR2022QD014).

Appendix A. Supplementary material

Supplementary data to this article can be found online at <https://doi.org/10.1016/j.compgeo.2023.105338>.

References

- Anagnostou, G., 1993. A model for swelling rock in tunneling. Rock Mech. Rock Eng. 26 (4), 307–331.
- Bai, C.H., Xue, Y.G., Qiu, D.H., Su, M.X., Ma, X.M., Liu, H.T., 2021. Analysis of factors affecting the deformation of soft rock tunnels by data envelopment analysis and a risk assessment model. Tunnel. Undergr. Space Technol. 116.
- Blackwell, T., Kennedy, J., 2019. Impact of communication topology in particle swarm optimization. IEEE Trans. Evol. Comput. 23 (4), 689–702.
- Cui, Z.D., Liu, D.A., Wu, F.Q., 2014. Influence of dip directions on the main deformation region of layered rock around tunnels. Bull. Eng. Geol. Environ. 73 (2), 441–450.
- Das, A.K., Mishra, D., Das, K., Mallick, P.K., Kumar, S., Zymbler, M., El-Sayed, H., 2022. Prophesying the short-term dynamics of the crude oil future price by adopting the survival of the fittest principle of improved grey optimization and extreme learning machine. Mathematics 10 (7).
- Di, Q., Li, P., Zhang, M., Wu, J., 2023. Influence of permeability anisotropy of seepage flow on the tunnel face stability. Undergr. Space 8, 1–14.
- Do, T.N., Wu, J.H., 2020. Simulation of the inclined jointed rock mass behaviors in a mountain tunnel excavation using DDA. Comput. Geotech. 117, 103249.
- Do, T.N., Wu, J.H., Lin, H.M., 2017. Investigation of Sloped Surface Subsidence during Inclined Seam Extraction in a Jointed Rock Mass Using Discontinuous Deformation Analysis. Int. J. Geomech. 17 (8).
- Fang, Q., Wang, G., Du, J., Liu, Y., Zhou, M., 2023. Prediction of tunnelling induced ground movement in clay using principle of minimum total potential energy. Tunn. Undergr. Space Technol.
- Feng, S., Dai, S., Lei, H., 2022. Application of an integrated nonuniform seismic random excitation method in tunnel engineering in soft soil areas. Comput. Geotech. 105043.
- Feng, W., Huang, R., Li, T., 2012. Deformation analysis of a soft-hard rock contact zone surrounding a tunnel. Tunn. Undergr. Space Technol. 32, 190–197.
- Fortsakis, P., Nikas, K., Marinos, V., Marinos, P., 2012. Anisotropic behaviour of stratified rock masses in tunnelling. Eng. Geol. 141–142, 74–83.
- Gao, F., Stead, D., Kang, H., 2014. Simulation of roof shear failure in coal mine roadways using an innovative udec trigon approach. Comput. Geotech. 61, 33–41.
- He, M., 2011. Physical modeling of an underground roadway excavation in geologically 45° inclined rock using infrared thermography. Eng. Geol. 121, 165–176.
- He, M., Jia, X., Gong, W., Faramarzi, L., 2010a. Physical modeling of an underground roadway excavation in vertically stratified rock using infrared thermography. Int. J. Rock Mech. Min. 47, 1212–1221.

- He, M.C., Gong, W.L., Zhai, H.M., Zhang, H.P., 2010b. Physical modeling of deep ground excavation in geologically horizontal strata based on infrared thermography. *Tunn. Undergr. Sp. Tech.* 25, 366–376.
- He, P., Xu, F., Sun, S., 2020. Nonlinear deformation prediction of tunnel surrounding rock with computational intelligence approaches. *Geomat. Nat. Haz. Risk* 11 (1), 414–427.
- Hoek, E., Guevara, R., 2009. Overcoming squeezing in the yacamb(a)-quibor tunnel, venezuela. *Rock Mech. Rock Eng.* 42 (2), 389–418.
- Jethwa, J.L., Singh, B., Singh, B., Mithal, R.S., 1980. Influence of geology on tunnelling conditions and deformational behavior of supports in faulted zones - a case history of the chhibro-khodri tunnel in india. *Eng. Geol.* 16 (3–4), 291–319.
- Jia, P., Tang, C.A., 2008. Numerical study on failure mechanism of tunnel in jointed rock mass. *Tunn. Undergr. Space Technol.* 23 (5), 500–507.
- Kou, H., He, C., Yang, W.B., Wu, F.Y., Zhou, Z.H., Meng, W., Xiao, L.G., 2022. Asymmetric deformation characteristics and mechanical behavior for tunnels in soft-hard inclined contact strata under high geo-stress: a case study. *Bull. Eng. Geol. Environ.* 81 (7).
- Li, C., Hou, S., Liu, Y., Qin, P., Jin, F., Yang, Q., 2020. Analysis on the crown convergence deformation of surrounding rock for double-shield tbm tunnel based on advance borehole monitoring and inversion analysis. *Tunn. Undergr. Space Technol.* 103, 103513.
- Li, Z., Xue, Y., Li, S., Qiu, D., Su, M., Zhao, Y., Zhou, B., 2019. An analytical model for surrounding rock classification during underground water-sealed caverns construction: a case study from eastern china. *Environ. Earth Sci.* 78 (20).
- Li, Y., Zhang, D., Fang, Q., Yu, Q., Xia, L., 2014. A physical and numerical investigation of the failure mechanism of weak rocks surrounding tunnels. *Comput. Geotech.* 61, 292–307.
- Li, P., Zhao, Y., Zhou, X., 2016. Displacement characteristics of high-speed railway tunnel construction in loess ground by using multi-step excavation method. *Tunn. Undergr. Space Technol.* 51, 41–55.
- Lin, P., Liu, H., Zhou, W., 2015. Experimental study on failure behaviour of deep tunnels under high in-situ stresses. *Tunn. Undergr. Space Technol.* 46, 28–45.
- Liu, W., Chen, J., Chen, L., Luo, Y., Shi, Z., Wu, Y., 2022. Nonlinear deformation behaviors and a new approach for the classification and prediction of large deformation in tunnel construction stage: a case study. *Eur. J. Environ. Civ. Eng.* 26 (5), 2008–2036.
- Mahdevari, S., Haghigat, H.S., Torabi, S.R., 2013. A dynamically approach based on svm algorithm for prediction of tunnel convergence during excavation. *Tunn. Undergr. Space Technol.* 38, 59–68.
- Meng, L., Li, T., Jiang, Y., Wang, R., Li, Y., 2013. Characteristics and mechanisms of large deformation in the zhegu mountain tunnel on the sichuan–tibet highway. *Tunn. Undergr. Space Technol.* 37, 157–164.
- Pandit, B., Sivakumar babu, G.L., 2021. Probabilistic stability assessment of tunnel-support system considering spatial variability in weak rock mass. *Comput. Geotech.* 137, 104242 <https://doi.org/10.1016/j.comgeo.2021.104242>.
- Panthi, K.K., Nilsen, B., 2007. Uncertainty analysis of tunnel squeezing for two tunnel cases from nepal himalaya. *Int. J. Rock Mech. Min. Sci.* 44 (1), 67–76.
- Qi, P.F., Chang, J.C., Chen, X., Wang, T., Wu, M.Y., 2022. Identification of rock properties of rock wall cut by roadheader based on pso-vmd-lssvm. *Front. Earth Sci.* 10.
- Shi, S.S., Zhao, R.J., Li, S.C., Xie, X.K., Li, L.P., Zhou, Z., Liu, H.L., 2019. Intelligent prediction of surrounding rock deformation of shallow buried highway tunnel and its engineering application. *Tunn. Undergr. Space Technol.* 90, 1–11.
- Shi, L., Zhou, H., Song, M., Lu, J., Liu, Z., 2021. Geomechanical model test for analysis of surrounding rock behaviours in composite strata. *J. Rock Mech. Geotech. Eng.* 13 (4), 774–786.
- Tao, Z., Cao, J., Yang, L., Guo, A., Huang, R., Yang, X., Yuan, D., Hou, L., 2020. Study on deformation mechanism and support measures of soft surrounding rock in muzhailing deep tunnel. *Adv. Civil Eng.* 2020, 1–14.
- Tien, Y.M., Kuo, M.C., Juang, C.H., 2006. An experimental investigation of the failure mechanism of simulated transversely isotropic rocks. *Int. J. Rock Mech. Min. Sci.* 43 (8), 1163–1181.
- Wu, J.H., Ohnishi, Y., Nishiyama, S., 2004. Investigation on block displacements due to a shallow tunnel excavation in an inclined brick-type jointed rock mass using discontinuous deformation analysis. *J. Chin. Inst. Eng.* 27 (3), 307–314.
- Xue, Y.G., Li, Z.Q., Qiu, D.H., Zhang, L.W., Zhao, Y., Zhang, X.L., Zhou, B.H., 2019. Classification model for surrounding rock based on the pca-ideal point method: an engineering application. *Bull. Eng. Geol. Environ.* 78 (5), 3627–3635.
- Xue, Y.G., Ma, X.M., Qiu, D.H., Yang, W.M., Li, X., Kong, F.M., Zhou, B.H., Qu, C.Q., 2021a. Analysis of the factors influencing the nonuniform deformation and a deformation prediction model of soft rock tunnels by data mining. *Tunn. Undergr. Space Technol.* 109.
- Xue, Y.G., Ma, X.M., Qiu, D.H., Yang, W.M., Li, X., Kong, F.M., Zhou, B.H., Qu, C.Q., 2021b. Analysis of the factors influencing the nonuniform deformation and a deformation prediction model of soft rock tunnels by data mining. *Tunn. Undergr. Space Technol.* 109, 103769.
- Xue, Y.G., Liu, H.T., Bai, C.H., Su, M.X., Qiu, D.H., Zhou, B.H., Yu, Y.H., Jiang, X.D., 2022. Extension prediction model of soft rock tunnel deformation grade based on entropy weight method and rough set. *Environ. Earth Sci.* 81 (1).
- Yang, S.Q., Chen, M., Fang, G., Wang, Y.C., Meng, B., Li, Y.H., Jing, H.W., 2018. Physical experiment and numerical modelling of tunnel excavation in slanted upper-soft and lower-hard strata. *Tunn. Undergr. Space Technol.* 82, 248–264.
- Yang, S., Tao, Y., Xu, P., Chen, M., 2019. Large-scale model experiment and numerical simulation on convergence deformation of tunnel excavating in composite strata. *Tunn. Undergr. Space Technol.* 94, 103133.
- Yertutanol, K., Akgün, H., Sopaci, E., 2020. Displacement monitoring, displacement verification and stability assessment of the critical sections of the konak tunnel, Izmir, turkey. *Tunn. Undergr. Space Technol.* 101, 103357.
- Yu, W.J., Pan, B., Zhang, F., Yao, S.F., Liu, F.F., 2019. Deformation characteristics and determination of optimum supporting time of alteration rock mass in deep mine. *KSCE J. Civ. Eng.* 23 (11), 4921–4932.
- Zhang, Q., Wang, H., Jiang, Y., Lu, M., Jiang, B., 2019. A numerical large strain solution for circular tunnels excavated in strain-softening rock masses. *Comput. Geotech.* 114, 103142.
- Zheng, H., Li, P., Ma, G., Zhang, Q., 2022. Experimental investigation of mechanical characteristics for linings of twins tunnels with asymmetric cross-section. *Tunn. Undergr. Space Technol.* 119.
- Zhou, J., Yang, X.A., 2021. Deformation behavior analysis of tunnels opened in various rock mass grades conditions in china. *Geomech. Eng.* 26 (2), 191–204.